

## VIBRONIC SPECTRA OF OXAZINE 750 DYE IN AQUEOUS MEDIA: A COMPUTATIONAL STUDY

Leontieva S.V.

Black Sea Higher Naval Orders of the Red Star School named after P.S. Nakhimov

Dybenko st., 1a, Sevastopol, 299028, Russia; e-mail: tezidi@gmail.com

Received 26.08.2023. DOI: 10.29039/rusjbp.2023.0643

**Abstract.** The MN12SX/6-31++G(d,p)/SMD theory level exactly reproduced both positions of the main maximum and short-wavelength shoulder of OX750 absorption in an aqueous solution. The optimal functional for calculating the vibronic absorption spectra of different oxazine dyes in an aqueous solution was discussed based on the author's present and previous studies. The absorption spectrum shoulder is caused by the vibronic transition. The vibrations involved in vibronic transitions correspond to large-scale molecular movements, are low-frequency, and very weak compared to the others. However, excitation significantly influences the vibrations including the most intensive ones. Photoinduced charge redistribution is local and there is no charge transfer over the dye molecule as a whole. Aliphatic hydrogen atoms prevent water molecules from accessing the N24 nitrogen atom. Considering H-bonded "solute-solvent" interactions by three water molecules led to a redshift of the entire spectrum by  $\approx 15$  nm. A strengthening of H-bonds with water molecules upon OX750 excitation was found, which explains this bathochromic effect. The intensity of low-frequency vibrations (including those involved in vibronic transitions) increases with the addition of bound water molecules, especially in an excited state. The vibration of the N-H bond of the imino group is strengthened (especially in an excited state) due to water molecule binding. Noticeable polarization of one water molecule bounded was revealed upon dye excitation. The vibronic model was also applied to calculate the emission spectrum of OX750 in the aqueous media.

**Key words:** TD-DFT/DFT, vibronic transitions, aqueous solution, oxazine 750, absorption spectrum, emission spectrum.

### INTRODUCTION

Oxazine 750 (OX750, Fig. 1) is a highly fluorescent dye used in lasers [1-4], as well as a fluorescent marker [5,6] and included in chemical sensors [7].

Using optical methods, it was found that OX750 can effectively bind to DNA [6], surfaces of sol-gel glasses [8], porous silicate xerogel monoliths [9], nanoporous crystals [10], silicate xerogel [11]. A fairly large number of experimental works are devoted to the study of the optical properties of the OX750 itself. The Zhou and Han group studied the fluorescence and relaxation of this dye in various organic solvents [12-14]. The solvatochromism of OX750 in water [15] and other isotropic solvents [16], hydrophilic gel [17], and also in anisotropic medium (liquid crystals) [18] was investigated by the group of Ghanadzadeh and Zakerhamidi. Solvent effects were also analyzed by Rauf and Zaman [19]. The two-photon absorption of the dye was studied in Refs. [20,21]. While lasers use alcoholic solutions of OX750, the application of a dye as a fluorescent marker and chemical sensor requires an aqueous environment. Therefore, a detailed description and understanding of the photoexcitation of the OX750 in the aquatic environment, which can be achieved through theoretical analysis, is important. However, the theoretical analysis of the photoexcitation and relaxation of the OX750 was performed only for a non-aqueous medium. A theoretical study of the fluorescence and vibrational relaxation of OX750 in acetone was performed using the perturbative density operator method and the transient linear susceptibility theory [22]. The above-mentioned group of Zhou and Han, using the TD-DFT and CIS methods, analyzed the intermolecular H-bonds of OX750 in the ground and excited states with two ethanol molecules, as well as the electron transfer between them [13]. According to their calculations, one of the alcohol molecules is bound with the oxygen atom of the dye, and the other with the nitrogen atom of the side aminoethyl group. In a later work by the same authors, the energies of OX750 H-bonds (oxygen and nitrogen atoms of the central ring) with various organic solvents (acetone, methanol, ethanol, DMF, DMSO, and formamide) and its atomic charges in excited states were calculated [12]. An important result of Refs. [12,13] is the discovery of the enhancement of the H-bonds of OX750 with the solvent upon excitation. It should be noted that these authors further elaborated in detail the influence of photoexcitation of a solute on its H-bonds with a solvent for many different systems (see their review [23]). At once, vertical electronic transitions in

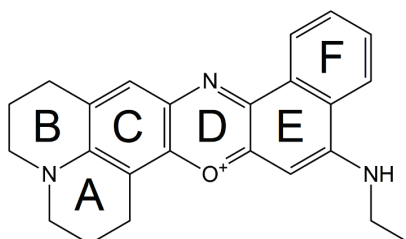


Figure 1. Chemical structure of OX750

Refs. [12,13] does not reproduce the experimental spectrum of OX750. For this purpose, it needs to consider vibronic transitions [24-27]. The absorption spectra of dilute OX750 solutions (both in water and in organic solvents) have a short-wavelength shoulder [12,17,18,20,21]. For an OX750 in aqueous media, the shoulder and the main maximum are situated at  $\lambda_{\text{shoulder}}=612$  nm and  $\lambda_{\text{max}}=666$  nm, respectively [21]. The authors of Refs. [17,18,21] believe that this shoulder is the dimer absorption band. However, a spectrophotometrically resolved spectrum of the OX750 monomer (Fig. 4) [21] has a shoulder also. In Ref. [20] authors state that the shoulder has a vibronic nature. It can also be caused by a separate electronic transition. The issue of the origin of the short-wavelength shoulder of the absorption spectra of dilute OX750 solutions can be answered by theoretical calculations of the OX750 excited states and vibronic transitions between them. This work completes a series of theoretical studies of oxazine dyes [28-33].

## METHODS

Let us briefly describe the quantum-chemical model of photoexcitation of a dye molecule in solution, which corresponds to the steady-state absorption spectroscopy experiment, by which the calculation results were verified.

When a photon is absorbed, the solute molecule, which was originally in the ground state (GS), goes into an excited non-equilibrium state, also called Franck-Condon (FC). This nonequilibrium is since, according to the Franck-Condon principle [34], the electronic transition first occurs at fixed  $R_{\text{GS}}$  positions of the nuclei (Fig. 2). The invariance of the coordinates corresponds to the vertical transition line  $E_{\text{vert}}$ , shown in yellow in Fig. 2.

The nonequilibrium of the excited electron shell and nuclei, whose  $R_{\text{GS}}$  coordinates still correspond to the ground state, leads to the activation of vibrational energy levels of the nuclear core (green wave in Fig. 2), so the transition is not purely electronic, but electronic-vibrational (vibronic). Since the excitation of the molecule under consideration occurs in solution, the reaction to it from the solvent (reaction field) will also initially be nonequilibrium. In this work, the nonequilibrium field of the solvent reaction was set using the state-specific approach [35]. A detailed modern interpretation of the Franck-Condon principle is given in Ref. [36].

From the excited Franck-Condon state, the solute molecule and the solvent molecules closest to it relax to the excited equilibrium state (EES) by changing the coordinates of the nuclei ( $R_{\text{GS}} \rightarrow R_{\text{EES}}$ , red arrow in Fig. 2) and polarization, respectively. This process was described by the equilibrium solvation model [37]. The difference between the respective energies is designated as the adiabatic energy:  $E_{\text{adia}}=E_{\text{EES}}-E_{\text{GS}}$  (see Fig. 2).

According to Kasha's rule [38], the emission originates from EES and is also a vertical transition (purple arrow in Fig. 2) following the Franck-Condon principle. In other words, the nuclear core remains in the configuration corresponding to the excited state ( $R_{\text{EES}}$ ), while the electron shell returns to its ground state. This mutual nonequilibrium of the nuclear core and the electron shell again leads to the activation of the vibrational energy levels of the nuclear core (turquoise wave in Fig. 2). Then the nuclear core relaxes to the basic configuration of the electron shell (blue arrow in Fig. 2), and the system returns to its GS. Unfortunately, the literature does not contain the emission spectrum of OX750 in an aqueous solution, there is only the magnitude of the emission maximum  $\lambda_{\text{em}}=667$  nm [16]. Therefore, the verification of the selected level of theory was carried out using the experimental absorption spectrum of the dye [21]. To avoid confusion, the calculation of the emission spectrum and its analysis are described separately in Appendix A.

The aqueous medium was modeled in two ways: implicit and combined. In the first part of the work, the approximation of a polarizable continuum (Integral Equation Formalism of Polarizable Continuum Model, IEFPCM, see review [39]) was used. Based on the experience of Refs. [29-33,40], IEFPCM calculations with radii and non-electrostatic terms of the SMD solvation model [41] were applied. Solvent continuum models consider site-specific interactions with the aqueous environment (i.e., strong hydrogen bonds) only on an average. As mentioned above, the OX750 molecule

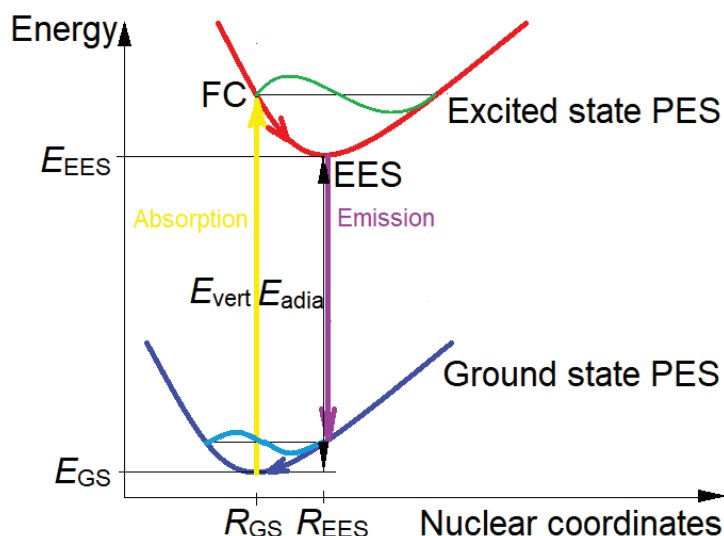


Figure 2. Energetic diagram of vibronic transitions

contains four H-bond donor and acceptor centers. To elucidate the effect of this strong hydrogen bonding, in the second part of the work, an explicit-implicit accounting of the aqueous medium was used: four water molecules strongly bound to dye molecules were specified explicitly, while the rest of the aqueous environment was implicitly specified.

In this work, the three lowest singlet electronic transitions in the OX750 molecule were analyzed. The PESs of the ground and excited states were calculated in the harmonic approximation near their minima,  $R_{GS}$  and  $R_{EES}$ , respectively. According to Ref. [36], anharmonicity effects are negligible for rigid and semirigid molecules (rotation of benzene rings relative to chromophores will be analyzed below). The PESs of the excited states were built using TD-DFT and the adiabatic Hessian model. The 6-31++G(d,p) basis set and forty hybrid functionals supported by Gaussian16 [42] were used in the work, among which one was chosen that gives the best match between the calculated vibronic absorption spectra and the experimental ones as the positions of the maxima ( $E_{\text{vibron}}=E_{\text{max}}$ ), and in shapes (see Results and Discussion).

Vibronic absorption spectra of dyes were calculated using the methodology [43] implemented in the Gaussian16 package based on time-independent DFT. The broadening of the vibronic transition bands was performed using Gaussians with  $\text{HWHM}=400\text{ cm}^{-1}$ , and the peaks of the calculated IR spectra - with  $\text{HWHM}=4\text{ cm}^{-1}$ . The temperature was assumed to be  $T=298\text{ K}$ . The spatial structure of the OX750 dye was taken from the PubChem database (CID 194254) and optimized as the ground state at the selected DFT level. Vibronic and IR spectra, spatial structures, molecular orbitals, distributions of electron density differences, and electrostatic potentials were built using the Gaussview6.0 package [44].

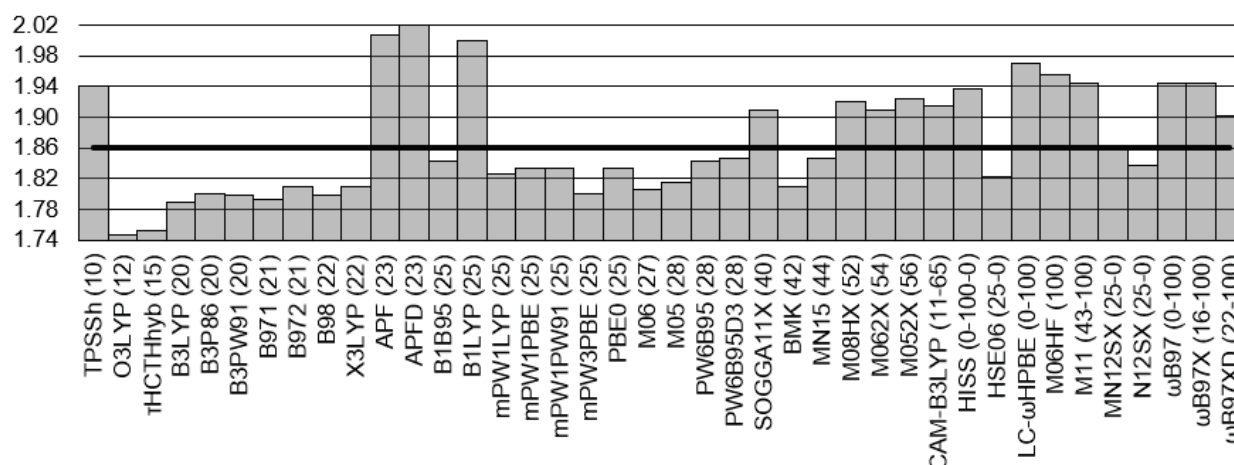
## RESULTS AND DISCUSSION

The energies of electronic states and transitions between them substantially depend on the X fraction of the "exact" Hartree-Fock exchange in the functional. As a rule, with an increase in the X value, the energy of the electronic (and vibronic) transition increases [45,46]. Pure functionals with  $X=0$  are not suitable for the analysis of excitation, since they often give too low (compared with experiment) transition energies and spurious excited states [47]. In the case of pronounced charge transfer, functionals with long-range correction should be used, in which the X value depends on the distance [48].

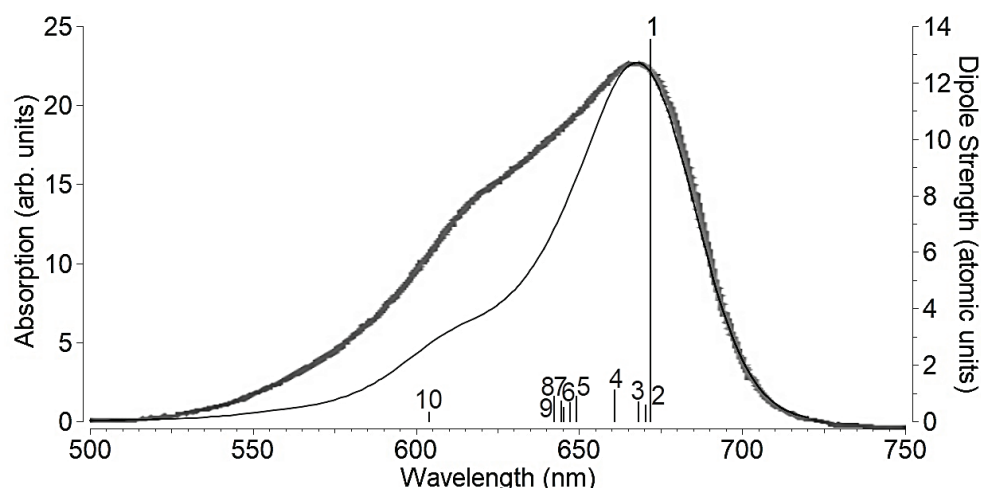
The main absorption peak in the visible spectrum region is caused by the HOMO→LUMO ( $S_0\rightarrow S_1$ ) transition [12,13]. Therefore, the selection of a hybrid functional, which reproduces the  $E_{\text{vibron}}$  (maximum of the calculated vibronic spectrum) for this transition coinciding with the main maximum  $E_{\text{max}}=1.86\text{ eV}$  (which corresponds to  $\lambda_{\text{max}}=666\text{ nm}$  [21]) of the resolved monomer spectrum of the dye (Fig. 3), was carried out.

From Fig. 3 it can be seen that the MN12SX functional [49] with long-range correction is in excellent agreement with the experiment on the position of the main maximum. MN12SX depends on the density, the density gradient, and the kinetic energy density. It includes an  $X=25\%$  at short-range distances and  $X=0\%$  (Hartree-Fock exchange is screened) at long-range ones. The success of the functional with a long-range correction may mean the presence of photoinduced charge transfer in the OX750 molecule. This assumption will be tested below by analysis of atomic charges. Note that both the MN12SX functional and SMD solvent model used in this study were developed by Truhlar's group.

The calculated spectrum coincides with the experimental one in terms of the positions of the main maximum and short-wavelength shoulder ( $\lambda_{\text{shoulder}}=612\text{ nm}$ , Fig. 4). The latter has a vibronic nature: it is due to vibronic transition #10 (see Fig. 4 and Table 1).



**Figure 3.** Maxima  $E_{\text{vibron}}$  (eV) of theoretical vibronic absorption spectra of OX750 in aqueous media. X percentage is indicated in parentheses. X values for small and large distances are indicated for functionals with long-range correction (HISS functional - for small, medium, and long distances, respectively). The bold horizontal line is the  $E_{\text{max}}$  value



**Figure 4.** The calculated vibronic absorption spectrum of OX750 in aqueous media (thin line) and resolved OX750 monomer spectrum in aqueous solution from Ref. [21] (thick line here and in Fig. 9, adapted with permission from AIP Publishing, order 5097060452897). The vertical lines are the dipole strength of the vibronic transitions (see Table 1)

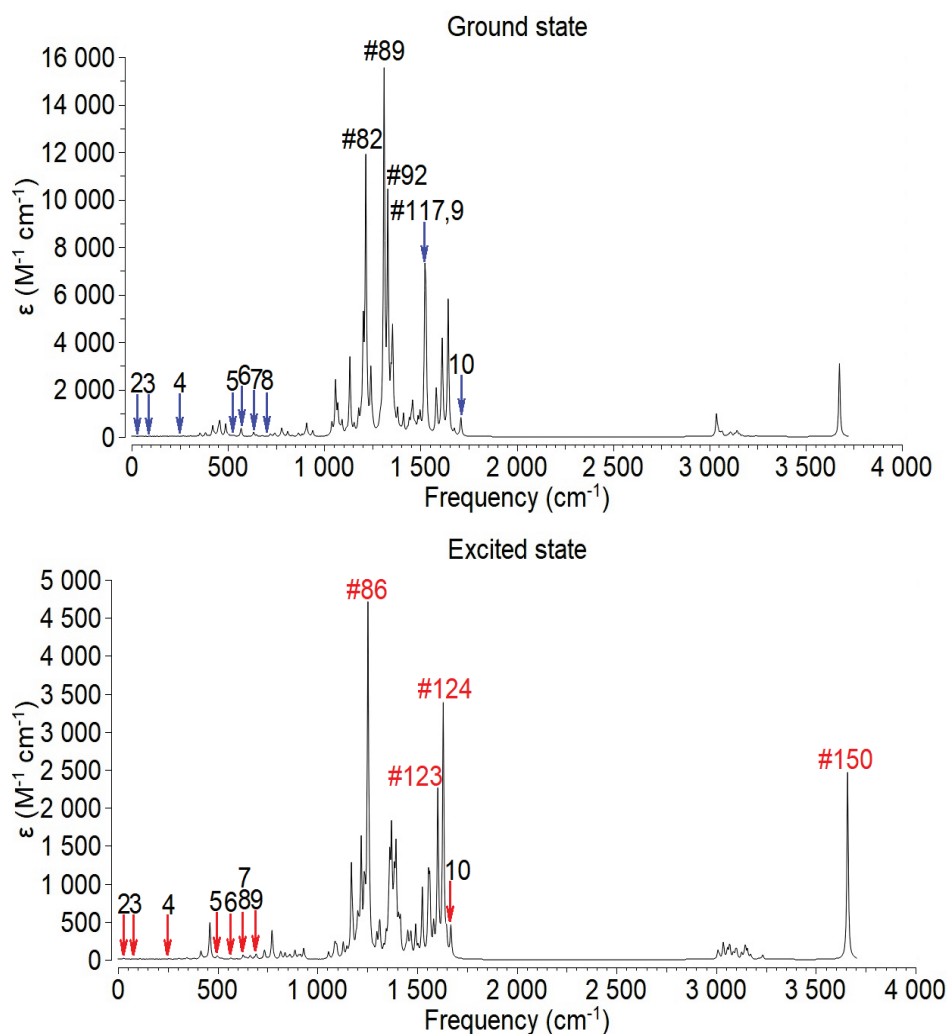
However, the shoulder in the calculated spectrum is twice lower than the experimental one. This may be due to both the dimeric absorption and the contribution of higher electronic transitions to the experimental spectrum. The latter assumption will be verified below.

Whilst, analysis of the OX750 excitation in an aqueous media will be performed below on the MN12SX/6-31++G(d,p)/SMD theory level. It should also be noted that the vibrations involved in vibronic transitions correspond to large-scale molecular movements, are low-frequency, and very weak compared to the others (Fig. 5).

**Table 1.** Parameters of OX750 vibronic transitions upon excitation in an aqueous media

#	Transition	$\lambda$ (nm)	E (eV)	$\nu$ ( $\text{cm}^{-1}$ )	I	p (atomic units)	Definitions of excited-state vibrations involved (see Fig. 5)
1	$0_0 \rightarrow 0^0$	672	1.85	0	167200	13.6	-
2	$0_0 \rightarrow 2^1$	670	1.85	29.2	6861	0.557	Flexural vibration of the chromophore perpendicular to its plane
3	$0_0 \rightarrow 5^1$	668	1.86	80.3	8383	0.678	Flexural vibration of the chromophore in its plane
4	$0_0 \rightarrow 15^1$	661	1.88	247	13760	1.10	Compression-stretching of the chromophore along its long axis
5	$0_0 \rightarrow 34^1$	649	1.91	520	11060	0.869	Compression-stretching of the central (heterocyclic) ring across the long axis of the chromophore
6	$0_0 \rightarrow 36^1$	647	1.92	567	8151	0.639	Compression-stretching of the central (heterocyclic) along the long axis of the chromophore
7	$0_0 \rightarrow 38^1$	645	1.92	613	6016	0.470	Compression-stretching of the side aromatic ring
8	$0_0 \rightarrow 39^1$	645	1.92	627	9107	0.711	Compression-stretching of the chromophore across its long axis
9	$0_0 \rightarrow 43^1$	642	1.93	684	11310	0.880	Shear vibration of the chromophore along its long axis
10	$0_0 \rightarrow 126^1$	604	2.05	1670	4317	0.316	Compression-stretching of the aromatic rings

$\lambda$  is the wavelength, E is the energy of the vibronic transition, I is the line intensity,  $\nu$  is the vibration frequency, and p is the dipole strength



**Figure 5.** Calculated IR spectra of OX750 in an aqueous media. The vibration frequencies of the excited state involved in absorption vibronic transitions are indicated by red arrows with appropriate numbers. Vibrations weakened by excitation are indicated by black numbers, and those enhanced by red. The vibration frequencies of the ground state involved in emission vibronic transitions are indicated by blue arrows with appropriate numbers

It is interesting to note that, according to our previous studies [28-33], the optimal functional (with the same 6-31++G(d,p) basis set and the SMD solvent model) for calculating the vibronic absorption spectrum of oxazine dyes in an aqueous solution depends on the number of chromophore rings. Thus, the chromophores of oxazine 1 [29], brilliant cresyl blue [30], and oxazine 4 [32] contain three rings, and the X3LYP functional gives the best agreement with the experiment for them. At the same time, for four- and six-ring chromophores, the optimal functional each time turns out to be different: M062X for cresyl violet [30],  $\omega$ B97XD for oxazine 170 (720) [31], O3LYP for the Nile red [28], and MN12SX for OX750 (this work). However, it should be clarified that, unlike the other dyes mentioned, Nile red is electrically neutral, and the 6-31G(d,p) basis set and the IEFPCM solvent model were used for it.

Comparing the calculated IR spectra of OX750 (see Fig. 5), one can see that excitation significantly influences the vibrations including the most intensive ones. The most significant photoinduced changes in oscillations are as follows. The mid-frequency fluctuations (#82, #89, #92, and #117) are noticeably weakened. Other mid-frequency vibrations (#86, #123, and #124) are greatly enhanced. All of the above modes describe the compression-stretching of the bonds of the chromophore in its plane in various combinations. Also, upon excitation, the most high-frequency vibration #150 (stretching-compression of the N-H bond of the imino group in the side chain (see Fig. 1) is significantly enhanced. The photoinduced changes in the vibration frequencies are small ( $\sim 25$   $\text{cm}^{-1}$ ). Visualization of all these vibrations is presented in Appendix as GIF files under the appropriate numbers. Changes in the vibration frequencies of OX750 due to excitation can also be visualized by the Duschinsky rotation matrix.

Two other electronic transitions in the visible spectrum region ( $S_0 \rightarrow S_2$  and  $S_0 \rightarrow S_3$ ) have a very low oscillator strength  $f$  (Table 2), and thus do not make an essential contribution to the absorption spectrum.

Frontier MOs involved in the  $S_0 \rightarrow S_1$  electronic transition considered are shown in Fig. 6. Their configurations are close to those obtained in Ref. [13] at the BP86/TZVP/vacuo theory level. From Fig. 6, it can be seen that the frontier MOs cover almost the entire molecule, with the least extent of the aliphatic rings and the side chain.

**Table 2.** Parameters of electronic states and transitions between them for OX750 in an aqueous media

Electronic state	$E_{eq}^*$ (eV)	Electronic transition	$\lambda_{adia}^{**}$ (nm)	$E_{adia}^{***}$ (eV)	$\lambda_{vert}$ (nm)	$E_{vert}$ (eV)	$\lambda_{vibron}$ (nm)	$E_{vibron}$ (eV)	f	Involved transitions
$S_0$ (GS)	-31769.92									
$S_1$	-31767.99	$S_0 \rightarrow S_1$	642	1.93	543	2.28	667	1.86	1.0775	HOMO $\rightarrow$ LUMO
$S_2$	-31767.24	$S_0 \rightarrow S_2$	463	2.68	428	2.90	461	2.69	0.0002	HOMO $\rightarrow$ (LUMO+1)
$S_3$	-31767.09	$S_0 \rightarrow S_3$	438	2.83	416	2.98	433	2.87	0.0569	(HOMO-1) $\rightarrow$ LUMO

\*equilibrium energy (PES minima, see Fig. 2)

\*\* $\lambda_{adia} = hc/E_{adia}$

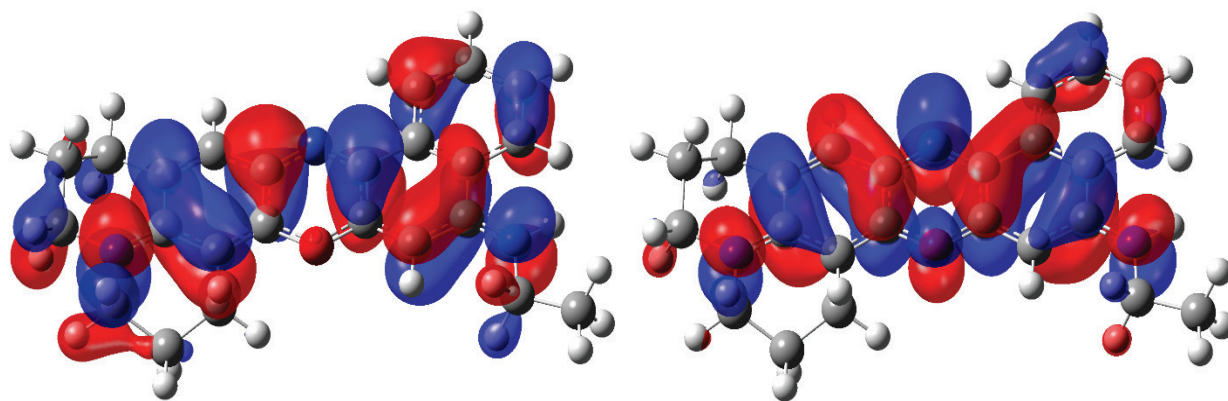
\*\*\* $E_{adia} = E_{EES} - E_{GS}$ , see Fig. 2

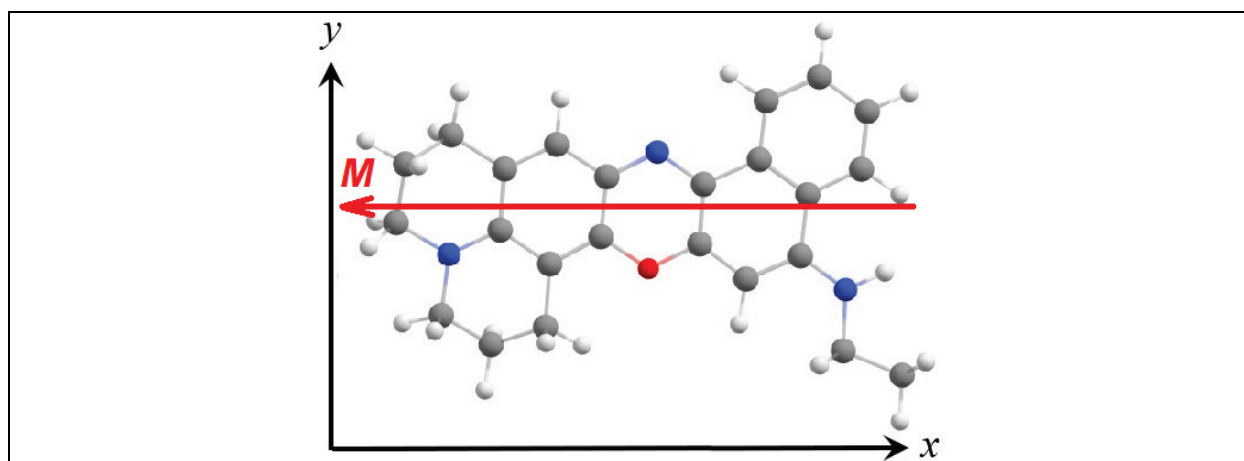
The OX750 dipole moment increases due to excitation ( $\mu_{GS} < \mu_{FC} \approx \mu_{EES}$ , Table 3). It corresponds to the  $\pi \rightarrow \pi^*$  type of electronic transition and redshift of absorption maximum with solvent polarity increases [50]. However, the OX750 does not show this dependence. In particular, solvents with donors of H-bonds cause a redshift of the OX750 absorption bands compared to 1,4-dioxane ( $\lambda_{max} = 649$  nm for dioxane, 665 nm for acetone, 669 nm for methanol, and 665 nm for water) [18]. Therefore, OX750 solvatochromism significantly influenced by specific solute-solvent H-bonds. In the present work, when simulating water molecules strongly bound to the dye, two of them were H-bond donors, and one was acceptor (Fig. 8), and they caused the redshift also (see below). In Ref. [16] based on solvatochromic shifts for polar solvents,  $\mu_{GS} = 3.7$  D and  $\mu_{EES} = 9.9$  D values were obtained. In Ref. [20], from solvatochromic shifts with H-bonding considering, the value  $\Delta\mu = \mu_{EES} - \mu_{GS} = (2.1 \pm 1.1)$  D was calculated. As you can see, these results significantly differ quantitatively, both among themselves and with the values obtained in the present work. The transition moment  $M$  is oriented almost along the long chromophore axis (see Scheme inside Table 3, the coordinate axes coincide along the OX750 principal inertia axes).

To estimate the photoinduced electron density shifts in OX750 cation, its Merz-Kollman [51] charges of non-hydrogen atoms were analyzed. In the GS, the positive charges are located mainly on the C6, C7, and C10 atoms, and the negative ones - are on N1, N5, C2, C4, and C9 atoms. Due to excitation, the GS  $\rightarrow$  FC transition leads to a significant increase in electron density at the N5 atom, and a decrease - at C4, C6, C10, and C12 atoms. Hereafter, the absolute values of  $\mu_x$ ,  $\mu_y$ , and  $\mu$  increase (see Table 3). The FC  $\rightarrow$  EES relaxation leads to an electron density decrease in the C12 and C21 atoms and an increase in the C11 atom. This causes a decrease of  $\mu_x$  and  $\mu_y$  modulus and an insignificant  $\mu$  increase. The electron density displacement during the GS  $\rightarrow$  FC vertical excitation is much stronger than upon the FC  $\rightarrow$  EES relaxation.

Photoinduced charge redistribution can be represented also by building a map of the difference in electron density (Fig. 7) or the distribution of electrostatic potential over the van der Waals surface of the molecule. As you can see from these Figs., charge redistribution is very complex (albeit local), and encompasses, to a greater or lesser extent, the entire dye molecule. Only the ethyl side group remains unused in this process. Thus, there is no charge transfer over the dye molecule as a whole.

To estimate the contribution of hydration to the OX750 excitation in an aqueous media, we calculated the vibronic absorption spectrum for the "OX750+3H<sub>2</sub>O" hydrated complex (Figs. 8 and 9). In Ref. [13], two ethanol molecules bind only to nitrogen molecules. In this work, it is shown that a water molecule (probably due to its smaller size) is also capable of binding to the endocyclic oxygen O8 atom (see the caption in Fig. 8). It should be noted that aliphatic hydrogen atoms

**Figure 6.** HOMO (left) and LUMO (right). Positive lobes are shown in red and negative lobes in blue

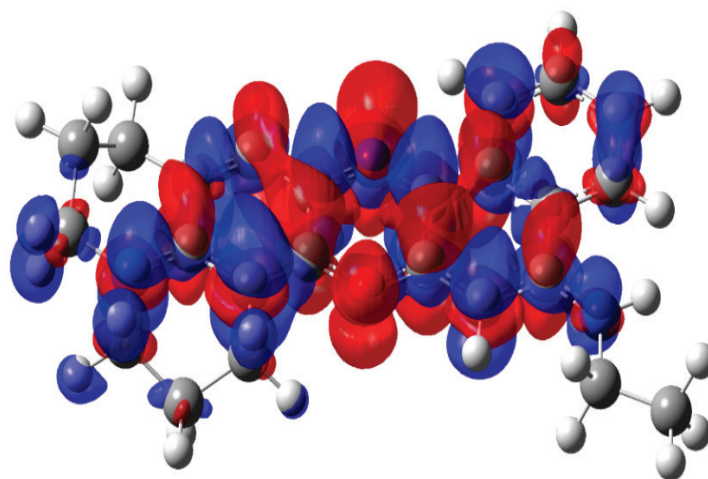
**Table 3.** Calculated moments (D) of OX750 cation in aqueous media (MN12SX/6-31++G(d,p)/SMD theory level)


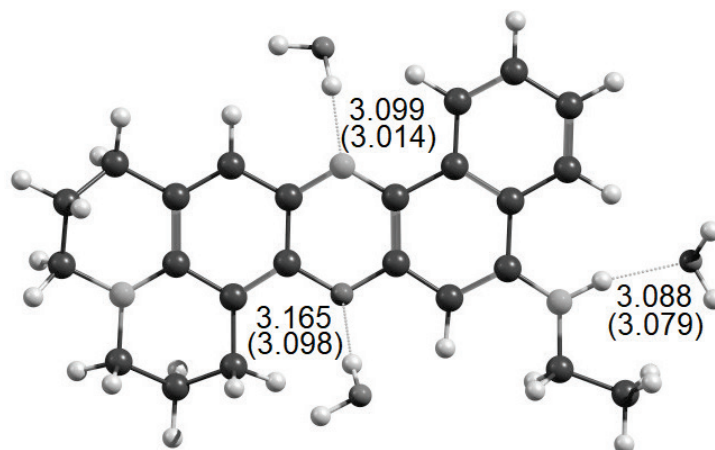
Dipole moment	Ground state ( $S_0$ )	Excited state ( $S_1$ )		Transition dipole moment	
		Franck-Condon	Equilibrium		
$\mu_x$	-1.45	-2.65	-2.70	$M_x$	-13.7
$\mu_y$	-5.13	-6.07	-6.12	$M_y$	0.0399
$\mu_z$	0.227	0.275	0.569	$M_z$	0.0615
$\mu$	5.34	6.63	6.72	$M$	13.7

prevent water molecules from accessing the N24 nitrogen atom. The ABC ring group of the OX50 molecule (see Fig. 1) is a julolidyl moiety that is part of 7-amino-substituted coumarins, for which H-bonding of water with a nitrogen atom is possible (see, for example, case of coumarin 102(480) in Ref. [52]). However, unlike coumarin 102, the OX750 julolidyl moiety does not have such a strong pucker, and the resulting displacement of aliphatic H-atoms (versus a flat structure) is insufficient for the guaranteed access of the water molecule to the nitrogen atom. Note that the aforementioned H-bond of coumarin 102 with a water molecule is weak and breaks upon excitation [52].

All three H-bonds of OX750 with water molecules in the excited equilibrium state are stronger than in the ground one, which is reflected in its shortening (see Fig. 8). As mentioned above (see Introduction), this feature took place for the OX750 in ethanol (theoretical study of Zhao and Han [13]). The absorption intensity decreases slightly when adding three explicit water molecules (cf. Figs. 4 and 9).

However, in this case, a small short-wavelength vibronic peak at 535 nm in the calculated spectrum appears, which is absent in the experimental spectrum. This artifact peak is caused by a bug in Gaussian software. The main bands of the vibronic absorption spectrum of the "OX750+3H<sub>2</sub>O" system have the same shape as for a single OX750 cation, but its absorption maximum is at  $\lambda_{\text{vibron}}=681$  nm, and the shoulder at  $\lambda_{\text{shoulder}}\approx 630$  nm, i.e. the spectrum is redshifted by  $\approx 15$  nm (Fig. 9). This regularity is easily explained as follows. Since the interactions with the water molecules for OX750 EES are stronger than in the GS, the PES of the EES drops lower than for a completely implicit consideration of the aqueous solution. The convergence of the PESs leads to a decrease in  $E_{\text{adia}}$  and  $E_{\text{vert}}$  (see Fig. 2), and, respectively, to an increase in  $\lambda_{\text{vibron}}$ .

**Figure 7.** The electron density difference between the Franck-Condon point and the ground state. Regions of positive values are shown in red and negative values in blue

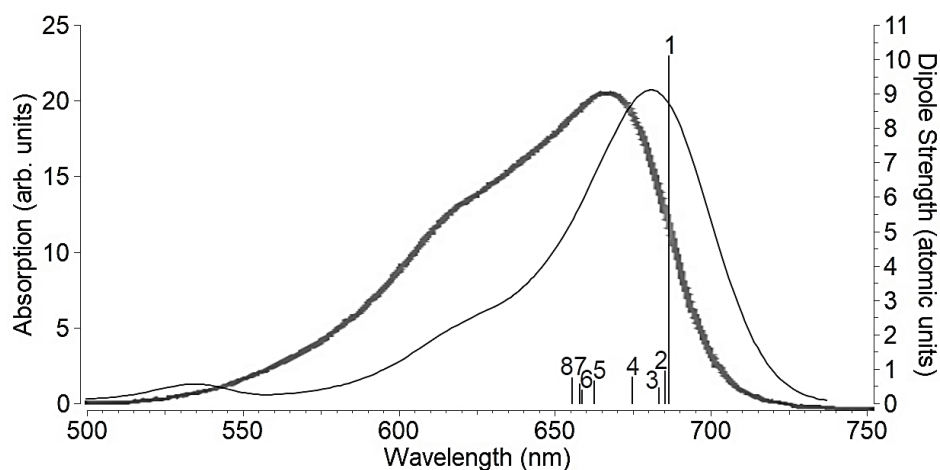


**Figure 8.** Calculated structure of the OX750 hydration complex with three water molecules. Strong H-bonds are shown with a dotted line. Their lengths in Å (distances between heavy atoms) are given for the ground and equilibrium excited (in parentheses) states. The water molecule bounded with the O8 atom (below in the Figure) is in front of the chromophore plane due to steric hindrances from the chromophore hydrogen atoms. The water molecule bounded with the N5 atom (above in the Figure) is located behind the plane of the chromophore for the same reason. The third water molecule is located in the plane of the chromophore

Let us analyze briefly the effect of strong H-bonds with water on the electronic and vibrational states of the dye. Changes in the vibronic transitions occur (cf. Figs. 4 and 9). Their number reduced from 10 to 8, and the transitions have varied essentially (cf. Table 1). The intensity of low-frequency vibrations (including those involved in vibronic transitions) increases with the addition of bound water molecules, especially in an excited state. IR spectra also changed. In particular, the normal modes of water molecules are added and vibration #150 of the N-H bond of the imino group is strengthened (especially in an excited state) due to water molecule binding (see Fig. 8). Frontier MOs of the "OX750+3H<sub>2</sub>O" complex practically coincide with those for a single OX750 molecule (cf. Fig. 6). It is interesting that out of three water molecules strongly bound to the OX750 cation, only one polarizes upon excitation (bound to the N5 endocyclic nitrogen atom, Fig. 10). As mentioned above, the electron density on the N5 atom increases the most. This leads to a significant charge redistribution of the water molecule bounded. It can also be visualized by the electrostatic potential distribution.

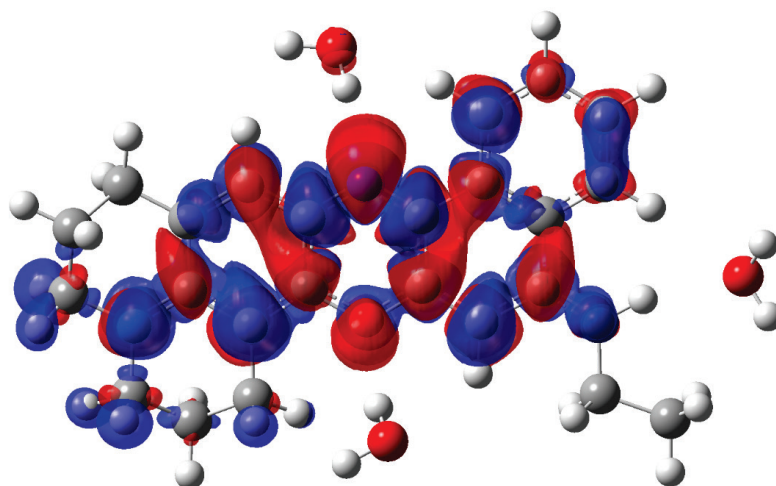
## CONCLUSIONS

The best agreement with the experiment on the position of the main maximum ( $\lambda_{\max} = 666$  nm) was given by MN12SX functional which contains a long-range correction. The MN12SX/6-31++G(d,p)/SMD theory level also exactly reproduced the position of the short-wavelength shoulder ( $\lambda_{\text{shoulder}} = 612$  nm). The optimal functional for calculating the vibronic absorption spectra of oxazine dyes in an aqueous solution depends on the number of chromophore rings. Thus, for the oxazines with three rings, the X3LYP functional gives the best agreement with the experiment. For four- and six-ring chromophores, the optimal functional each time turns out to be different. The vibrations involved in vibronic



**Figure 9.** The calculated vibronic absorption spectrum of the "OX750+3H<sub>2</sub>O" system (thin line) and the resolved monomer spectrum of OX750 aqueous solution from Ref. [21] (thick line)





**Figure 10.** The electron density difference between the Franck-Condon point and the ground state for the "OX750+3H<sub>2</sub>O" hydrated complex

transitions correspond to large-scale molecular movements, are low-frequency, and very weak compared to the others. Excitation significantly influences the vibrations including the most intensive ones. Aliphatic hydrogen atoms prevent water molecules from accessing the N24 nitrogen atom. Explicit consideration of strong H-bonds between waters and dye cation leads to an entire spectrum redshift by  $\approx 15$  nm. Strengthening of these H-bonds due to OX750 excitation was found, which explains this redshift. The intensity of low-frequency vibrations (including those involved in vibronic transitions) increases with the addition of bound water molecules, especially in an excited state. The vibration of the N-H bond of the imino group is strengthened (especially in an excited state) due to water molecule binding. Noticeable polarization of one out of three waters was revealed upon dye excitation.

#### References:

1. Eilenberger D.J., Isaacs E.D., Aumiller G.D. Near infrared, tunable, oxazine 750 perchlorate, synchronously-pumped picosecond ring dye laser. *Optics Commun.*, 1983, vol. 44, pp. 350-352.
2. Scheps R. Near-IR Dye Laser for Diode-Pumped Operation, *IEEE J. Quantum Electronics*, 1995, vol. 31, pp. 126-134.
3. Bos F. Optimization of spectral coverage in an eight-cell oscillator-amplifier dye laser pumped at 308 nm. *Appl. Optics*, 1981, vol. 20, pp. 3553-3556.
4. Fehrenbach G.W., Gruntz K.J., Ulbrich R.G. Subpicosecond light pulses from a synchronously modelocked dye laser with composite gain and absorber medium. *Appl. Phys. Lett.*, 1978, vol. 33, pp. 159-160.
5. Kaneta T., Imasaka T. Indirect Detection of Aromatic Hydrocarbons by Semiconductor Laser Fluorometry in Micellar Electrokinetic Chromatography. *Anal. Chem.*, 1995 vol. 67, pp. 829-834.
6. Shapiro H.M., Stephens S. Flow Cytometry of DNA Content Using Oxazine 750 or Related Laser Dyes With 633 nm Excitation. *Cytometry*, 1986, vol. 7, pp. 107-110.
7. Blyler L.L., Lieberman R.A., Cohen L.G., Ferrara J.A., Macchesney J.B. Optical Fiber Chemical Sensors Utilizing Dye-Doped Silicone Polymer Claddings. *Polym. Eng. Sci.*, 1989, vol. 29, pp. 1215-1218.
8. Sathy P., Penzkofer A. Absorption and fluorescence spectroscopic analysis of rhodamine 6G and oxazine 750 in porous sol-gel glasses. *J. Photochem. Photobiol. A*, 1997, vol. 109, pp. 53-57.
9. Ammer F., Penzkofer A., Weidner P. Concentration-dependent fluorescence behaviour of oxazine 750 and rhodamine 6G in porous silicate xerogel monoliths. *Chem. Phys.*, 1995, vol. 192, pp. 325-331.
10. Wark M., Ganschow M., Schulz-Ekloff G., Woehrl D. Incorporation of organic dye molecules in nanoporous crystals for the development of hexagonal solid state microlasers. *Proc. SPIE*, 2001, vol. 4456, pp. 57-67.
11. Weidner P., Penzkofer A. Picosecond transient spectral hole-burning studies on oxazine 750 in a silicate xerogel. *Chem. Phys.*, 1995, vol. 191, pp. 303-319.
12. Zhou P., Song P., Liu J.-Y., Shi Y., Han K., He G. Rotational Reorientation Dynamics of Oxazine 750 in Polar Solvents. *J. Phys. Chem. A*, 2008, vol. 112, pp. 3646-3655.
13. Zhao G.-J., Liu J.-Y., Zhou L.-C., Han K.-L. Site-Selective Photoinduced Electron Transfer from Alcoholic Solvents to the Chromophore Facilitated by Hydrogen Bonding: A New Fluorescence Quenching Mechanism. *J. Phys. Chem. B*, 2007, vol. 111, pp. 8940-8945.
14. Zhou L.-C., Shi Y., Liu J.-Y., Han K.-L. The effect of hydrogen-bond in alcoholic solvent on the solvation ultrafast dynamics of oxazine 750 dye. *Chin. Sci. Bull.*, 2008, vol. 53, pp. 1951-1954.
15. Milanchian K., Tajalli H., Ghanadzadeh A., Zakerhamidi M.S. Nonlinear optical properties of two oxazine dyes in aqueous solution and polyacrylamide hydrogel using single beam Z-scan. *Opt. Mater.*, 2009, vol. 32, pp. 12-17.
16. Zakerhamidi M.S., Golghasemi Sorkhabi S. Solvent effects on the molecular resonance structures and photo-physical properties of a group of oxazine dyes. *J. Luminesc.*, 2015, vol. 157, pp. 220-228.

17. Zakerhamidi M.S., Tajalli H., Ghanadzadeh A., Milanchian K., Hosseini Nasab N., Moghadam M. Effect of polyacrylamide hydrophilic gel composition on photo-physical behavior of Oxazine 750. *Spectrochim. Acta A*, 2010, vol. 77, pp. 164-169.
18. Ghanadzadeh A., Tajalli H., Zirack P., Shirdel J. On the photo-physical behavior and electro-optical effect of oxazine dyes in anisotropic host. *Spectrochim. Acta A*, 2004, vol. 60, pp. 2925-2932.
19. Rauf M.A., Zaman M.Z. Spectral properties of oxazines in various solvents. *Spectrochim. Acta A*, 1987, vol. 43, p. 1171.
20. Beuerman E., Makarov N., Drobizhev M., Rebane A. Justification of two-level approximation for description of two-photon absorption in oxazine dyes. *Proc. SPIE*, 2010, vol. 7599, pp. 75-99.
21. Yamaguchi S., Tahara T. Determining electronic spectra at interfaces by electronic sum frequency generation: One- and two-photon double resonant oxazine 750 at the air/water interface. *J. Chem. Phys.*, 2006, vol. 125, p. 194711.
22. Dong L.-Q., Niu K., Cong S.-L. Theoretical Analysis of Femtosecond Fluorescence Depletion Spectra and Vibrational Relaxations of Dye Oxazine 750 and Rhodamine 700 Molecules in Acetone Solution. *Int. J. Quantum Chem.*, 2007, vol. 107, pp. 1205-1214.
23. Zhao G.-J., Han K.-L. Hydrogen Bonding in the Electronic Excited State. *Acc. Chem. Res.*, 2012, vol. 45, pp. 404-413.
24. Jacquemin D., Brymond E., Planchat A., Ciofini I., Adamo C. TD-DFT vibronic couplings in anthraquinones: from basis set and functional benchmarks to applications for industrial dyes. *J. Chem. Theory Comput.*, 2011, vol. 7, pp. 1882-1892.
25. Lopez G.V., Chang C.-H., Johnson P.M., Hall G.E., Sears T.J., Markiewicz B., Milan M., Teslja A. What Is the Best DFT Functional for Vibronic Calculations? A Comparison of the Calculated Vibronic Structure of the  $S_1-S_0$  Transition of Phenylacetylene with Cavity Ringdown Band Intensities. *J. Phys. Chem. A*, 2012, vol. 116, pp. 6750-6758.
26. Charaf-Eddin A., Planchat A., Mennucci B., Adamo C., Jacquemin D. Choosing a Functional for Computing Absorption and Fluorescence Band Shapes with TD-DFT. *J. Chem. Theory Comput.*, 2013, vol. 9, pp. 2749-2760.
27. Jacquemin D., Bremond E., Ciofini I., Adamo C. Impact of Vibronic Couplings on Perceived Colors: Two Anthraquinones as a Working Example. *J. Phys. Chem. Lett.*, 2012, vol. 3, pp. 468-471.
28. Kostjukova L.O., Leontieva S.V., Kostjukov V.V. The Vibronic Absorption Spectrum and Electronic States of Nile Red in Aqueous Solution. *ChemistrySelect*, 2021, vol. 6, pp. 1297-1304.
29. Yaroshenko N.S., Kostjukova L.O., Kostjukov V.V. Excited states of six oxazine 1 conformers in aqueous solution: TD-DFT/DFT study. *J. Mol. Liquids*, 2021, vol. 341, p. 117456.
30. Kostjukov V.V. Photoexcitation of brilliant cresyl blue dye in aqueous solution: TD-DFT study. *Mol. Phys.*, 2021, pp. 66-47.
31. Kostjukov V.V. Photoexcitation of oxazine 170 dye in aqueous solution: TD-DFT study. *J. Mol. Model*, 2021, vol. 27, p. 311.
32. Kostjukov V.V. Photoexcitation of oxazine 4 dye in aqueous solution: TD-DFT study. *Chem. Phys.*, 2022, vol. 553, p. 111399.
33. Kostjukov V.V. Photoexcitation of cresyl violet dye in aqueous solution: TD-DFT study. *Theor. Chem. Acc.*, 2021, vol. 140, p. 155.
34. Condon E.U. Nuclear motions associated with electron transitions in diatomic molecules. *Phys. Rev.*, 1928, vol. 32, pp. 858-872.
35. Improta R., Barone V., Scalmani G., Frisch M.J. A state-specific polarizable continuum model time dependent density functional theory method for excited state calculations in solution. *J. Chem. Phys.*, 2006, vol. 125, p. 54103.
36. Alia J.D., Flack J.A. Unspecified verticality of Franck-Condon transitions, absorption and emission spectra of cyanine dyes, and a classically inspired approximation. *RSC Adv.*, 2020, vol. 10, pp. 43153-43167.
37. Scalmani G., Frisch M.J., Mennucci B., Tomasi J., Cammi R., Barone V. Geometries and properties of excited states in the gas phase and in solution: Theory and application of a time-dependent density functional theory polarizable continuum model. *J. Chem. Phys.*, 2006, vol. 124, p. 94107.
38. Kasha M. Characterization of electronic transitions in complex molecules. *Discuss. Faraday Soc.*, 1950, vol. 9, pp. 14-19.
39. Tomasi J., Mennucci B., Cammi R. Quantum mechanical continuum solvation models. *Chem. Rev.*, 2005, vol. 105, pp. 2999-3093.
40. Fleming S., Mills A., Tuttle T. Predicting the UV-vis spectra of oxazine dyes, Beilstein *J. Org. Chem.*, 2011, vol. 7, pp. 432-441.
41. Marenich A.V., Cramer C.J., Truhlar D.G. Universal solvation model based on solute electron density and a continuum model of the solvent defined by the bulk dielectric constant and atomic surface tensions. *J. Phys. Chem. B*, 2009, vol. 113, pp. 6378-6396.
42. Frisch M.J. et al. Gaussian 16, Revision C.01, Inc., Wallingford CT, 2016.
43. Baiardi A., Bloino J., Barone V. General Time Dependent Approach to Vibronic Spectroscopy Including Franck-Condon, Herzberg-Teller, and Duschinsky Effects. *J. Chem. Theory Comput.*, 2013, vol. 9, pp. 4097-4115.
44. Dennington R., Keith T.A., Millam J.M. GaussView Version 6.1, Semicem Inc., Shawnee Mission KS, 2016.
45. Dierksen M., Grimme S. The Vibronic Structure of Electronic Absorption Spectra of Large Molecules: A Time-Dependent Density Functional Study on the Influence of "Exact" Hartree-Fock Exchange. *J. Phys. Chem. A*, 2004, vol. 108, pp. 10225-10237.

46. Kantchev E.A.B., Norsten T.B., Sullivan M.B. Time-dependent density functional theory (TDDFT) modelling of Pechmann dyes: from accurate absorption maximum prediction to virtual dye screening. *Org. Biomol. Chem.*, 2012, vol. 10, pp. 6682-6692.
47. Escudero D., Laurent A.D., Jacquemin D. Time-dependent density functional theory: A tool to explore excited states. *Springer Int. Publish. Switzerland*, 2017, pp. 927-961.
48. Iikura H., Tsuneda T., Yanai T., Hirao K. A long-range correction scheme for generalized-gradient-approximation exchange functionals. *J. Chem. Phys.*, 2001, vol. 115, pp. 3540-3544.
49. Peverati R., Truhlar D.G. Screened-exchange density functionals with broad accuracy for chemistry and solid-state physics. *Phys. Chem.*, 2012, vol. 14, pp. 16187-16191.
50. Reichardt C. Solvatochromic Dyes as Solvent Polarity Indicator. *Chem. Rev.*, 1994, vol. 94, pp. 2319-2358.
51. Singh U.C., Kollman P.A. An approach to computing electrostatic charges for molecules. *J. Comput. Chem.*, 1984, vol. 5, pp. 129-145.
52. Hessz D., Hegely B., Kallay M., Vidoczy T., Kubinyi M. Solvation and Protonation of Coumarin 102 in Aqueous Media: A Fluorescence Spectroscopic and Theoretical Study. *J. Phys. Chem. A*, 2014, vol. 118, pp. 5238-5247.
53. Lakowicz J.R., Masters B.R. Principles of Fluorescence Spectroscopy. *Optics*, 2008, vol. 13.2, p. 29901.
54. Marciniak H., Hristova S., Deneva V., Kamounah F.S., Hansen P.E., Lochbrunner S., Antonov L. Dynamics of excited state proton transfer in nitro substituted 10-hydroxybenzo [h] quinolones. *Phys. Chem.*, 2017, vol. 19, pp. 26621-26629.
55. Greiner J., Sundholm D. Calculation of vibrationally resolved absorption and fluorescence spectra of the rylenes. *Phys. Chem.*, 2020, vol. 22, pp. 2379-2385.

### ВИБРОННЫЕ СПЕКТРЫ КРАСИТЕЛЯ ОКСАЗИНА 750 В ВОДНОМ РАСТВОРЕ: РАСЧЕТНОЕ ИССЛЕДОВАНИЕ

Леонтьева С.В.

Черноморское Высшее Военно-морское Ордена Красной Звезды Училище имени П.С. Нахимова

Дыбенко 1а, 299028, Россия; e-mail: tezidi@gmail.com

Поступила в редакцию 26.08.2023. DOI: 10.29039/rusjbpс.2023.0643

**Аннотация.** Уровень теории MN12SX/6-31++G(d,p)/SMD точно воспроизводит как положение основного максимума, так и коротковолнового плеча поглощения ОХ750 в водном растворе. На основе настоящих и предыдущих исследований автора выбран оптимальный функционал для расчета вибронных спектров поглощения различных оксазиновых красителей в водном растворе. Плечо спектра поглощения обусловлено вибронным переходом. Колебания, участвующие в вибронных переходах, соответствующие крупномасштабным молекулярным движениям, являются низкочастотными и очень слабыми по сравнению с остальными. Однако возбуждение существенно влияет на колебания, в том числе наиболее интенсивные. Фотоиндуцированное перераспределение заряда носит локальный характер и перенос заряда по молекуле красителя в целом отсутствует. Алифатические атомы водорода не позволяют молекулам воды получить доступ к атому азота N24. Учет взаимодействий «растворенное вещество-растворитель» по водородным связям трех молекул воды привел к красному смещению всего спектра на  $\approx 15$  нм. Обнаружено усиление водородных связей с молекулами воды при возбуждении ОХ750, что и объясняет такой батохромный эффект. Интенсивность низкочастотных колебаний (в том числе участвующих в вибронных переходах) возрастает при присоединении связанных молекул воды, особенно в возбужденном состоянии. Колебания связи N-H иминогруппы усиливаются (особенно в возбужденном состоянии) за счет связывания молекул воды. При возбуждении красителя обнаружена заметная поляризация одной связанной молекулы воды. Вибронная модель была также применена для расчета спектра излучения ОХ750 в водной среде.

**Ключевые слова:** TD-DFT/DFT, вибронные переходы, водный раствор, оксазин 750, спектр поглощения, спектр испускания.